Strongly nonlinear wave dynamics of continuum phononic materials with periodic rough contacts

Ganesh U. Patil* and Kathryn H. Matlack†

Department of Mechanical Science and Engineering, University of Illinois Urbana-Champaign, Urbana, Illinois 61801, USA

(Received 26 October 2021; revised 11 January 2022; accepted 19 January 2022; published 7 February 2022)

We investigate strongly nonlinear wave dynamics of continuum phononic material with discrete nonlinearity. The studied phononic material is a layered medium such that the elastic layers are connected through contact interfaces with rough surfaces. These contacts exhibit nonlinearity by virtue of nonlinear mechanical deformation of roughness under compressive loads and strong nonlinearity stemming from their inability to support tensile loads. We study the evolution of propagating Gaussian tone bursts using time-domain finite element simulations. The elastodynamic effects of nonlinearly coupled layers enable strongly nonlinear energy transfer in the frequency domain by activating acoustic resonances of the layers. Further, the interplay of strong nonlinearity and dispersion in our phononic material forms stegotons, which are solitarylike localized traveling waves. These stegotons satisfy properties of solitary waves, yet exhibit local variations in their spatial profiles and amplitudes due to the presence of layers. We also elucidate the role of rough contact nonlinearity on the interrelationship between the stegoton parameters as well as on the generation of secondary stegotons from the collision of counterpropagating stegotons. The phononic material exhibits strong acoustic attenuation at frequencies close to (and fractional multiples of) layer resonances, whereas it causes energy propagation as stegotons for other frequencies. This study sheds light on the wave phenomena achievable in continuum periodic media with local nonlinearity, and opens opportunities for advanced wave control through discrete and local contact nonlinearity.

DOI: 10.1103/PhysRevE.105.024201

I. INTRODUCTION

Nonlinearity is ubiquitous and exists in all disciplines of physics, from optics [1], chemistry [2], biology [3], thermodynamics [4], and material science [5] to cosmology [6], and even at various length scales. These physical nonlinearities have enabled advanced functionalities in engineering applications [7,8] and recently received great attention in enriching the dynamics of periodic media [9,10]. Specific to periodic *mechanical* systems, nonlinearity has enabled behaviors such as amplitude-dependent dynamic response [11–13], energy transfer between frequencies [14], nonreciprocity [15], supratransmission [16], and many more (see the review of [17]), not possible with linear media. Yet, most of these nonlinear studies were focused on pure discrete or continuum periodic systems. However, the hybrid nature of discrete nonlinearity in a continuum, which holds the potential for further enhancing the nonlinear wave dynamics, is relatively unexplored.

One of the revolutionary nonlinear behaviors studied in periodic media is the propagation of solitons or solitary waves, which are localized traveling waves, meaning they have a spatially localized (or compact) profile that travels through the system. Following Russell's observation of shallow-water waves [18] that maintained their shape and speed for a very long distance, characteristics of solitary waves have been extensively studied across various domains of science [11,19–21]. The formation of solitary waves is a result of the counterbalance between nonlinearity and dispersion. Recent progress on realizing these waves in phononic materials has led to numerous applications such as diodes [22], sound bullets [23], impact mitigators [24], robotic motion [25], and sensors [26]. Solitary waves have been studied in granular crystals [11,13,27–29], tensegrity structures [30], and bistable [31] and soft architecture [22,25,32], all of which were assumed as lumped-mass periodic systems, i.e., discrete nonlinearity connecting discrete particle masses. A few studies have explored the propagation of solitary waves in bilayered phononic media with material [33] or geometric [34] nonlinearity. Yet, it is an open question whether solitary waves exist in a continuum with periodic and discrete nonlinearity.

Moreover, the system architecture itself governs the nature of solitary waves that propagate through it. For example, phononic media supporting single polarization form scalar [13] solitary waves whereas media with coupled polarization support propagation of vector [22,32,33] solitary waves. A couple of other studies on nonlinear phononic materials have reported the formation and propagation of nanopterons [35] and stegotons [36]. These two solitarylike localized traveling waves arise from a unique interplay of the underlying periodic system and nonlinearity, and exhibit different characteristics than classical solitons. For example, nanopterons are solitary waves on top of small oscillations as observed in stacked woodpile structures with Hertzian contact nonlinearity [35] whereas stegotons are solitary waves with a roof-type (or stepwise) profile as reported in bilayered media with exponential material nonlinearity [36]. Clearly, the complex nonlinear wave dynamics is an effect of how nonlinearity is embedded and interacts with the underlying phononic system. In this

*gupatil2@illinois.edu
†kmatlack@illinois.edu

work, we study wave dynamics of a layered phononic material where the linear continua (or layers) are nonlinearly coupled. The focus of the study is to understand the role of strongly nonlinear coupling on the elastodynamic behavior of linear layers and the existence and propagation of localized traveling waves in such media. Additionally, we investigate how energy is distributed and exchanged within this architecture, where nonlinearity exists only at discrete locations separated by linear continua. Such understanding is crucial for these materials to be used for controlling the propagation of mechanical wave energy.

We take inspiration from the nonlinear dynamics of naturally occurring geomaterials [37]. Geomaterials offer nonlinear physical sources in the form of heterogeneous grains, pores, and microcracks. Despite rich nonlinear responses, these microstructural features are not yet explored in the context of engineered periodic media. We are interested in studying wave propagation through elastic media with these microstructures, but intentionally architected periodically. Specifically, we focus on periodic rough contacts, inspired by microcracks in geomaterials. Microcracks with rough surfaces are formed inside materials due to cyclic loading and thus have been investigated in the field of nondestructive evaluation as a parameter to indicate material damage [38]. Taking motivation from these applications, we are exploring wave propagation characteristics of periodic rough contacts—an architecture representative of nonlinearly coupled elastic layers. In our previous work [39], we revealed that the *weak* nonlinear interaction of the fundamental wave with *precompressed* rough contacts generates zero, second harmonic, and self-demodulated frequency waves. The amplitudes of these nonlinearly generated frequencies depend on (1) dispersion arising from the periodic arrangement of contacts and (2) local coupling of contacts with the surrounding continuum.

In this work, we investigate *strongly* nonlinear wave dynamics of the phononic material studied in our previous work [39]. The one-dimensional (1D) nonlinear phononic material is such that the periodicity is architected in the form of contact interfaces with rough surfaces, connecting finite thickness linear elastic layers. The *uncompressed* contacts exhibit strong nonlinearity stemming from their inability to support tensile loads. This is in addition to nonlinear contact response under compressive loads arising from nonlinear mechanical deformation of roughness. We study the evolution of propagating waves, excited in the form of Gaussian tone burst at frequencies on the same order as the modal frequencies of individual layers, using time-domain finite element (FE) simulations. Particularly, we illustrate the elastodynamics effects arising from the nonlinearly coupled layers and investigate the existence and properties of localized traveling waves in such phononic materials. The main objective of the paper is to report nonlinear wave phenomena of energy transfer through acoustic resonances and emergence of stegotons in continuum phononic materials with discrete contact nonlinearity, and present some insights through extensive numerical simulations.

The organization of the paper is as follows: In Sec. II, we discuss rough contact nonlinearity and a continuum phononic material model with periodic contacts. Our FE model for the analysis of strongly nonlinear wave propagation is also described. We then present strongly nonlinear responses of the phononic material in Sec. III. Nonlinearly activated layer resonances are described first, followed by the characteristics and collision dynamics of localized traveling waves. Finally, we conclude in Sec. IV and discuss open questions in this less explored domain for future investigations.

II. MATERIAL MODEL

A. Strongly nonlinear rough contacts

Rough contacts are defined as interfaces between rough surfaces, and they exhibit a nonlinear response due to the nonlinear mechanical deformation of contact asperities (unevenness of rough surfaces) under compressive loads [Fig. 1(a)]. At wavelengths much larger than these asperity sizes and assuming negligible interfacial mass, rough contacts can be treated as nonlinear springs through a quasistatic model approach [40]. Based on this model, a stiffness-pressure relation at the precompressed interface of two aluminum blocks with rough surfaces was obtained experimentally [40], which was later expanded asymptotically to eventually derive a nonlinear relationship between the contact pressure, $p(\Delta u)$, and displacement, Δu [41]. The nonlinear relation follows a power-law dependence [41] as given by

$$p(\Delta u) = \begin{cases} \left[p_0^{1-\beta} - (1-\beta)C(\Delta u - \delta_0)\right]^{1/(1-\beta)}, & \beta \neq 1 \\ p_0 \exp\left[-C(\Delta u - \delta_0)\right], & \beta = 1, \end{cases} \tag{1}$$

where C and β are curve fitting parameters of the experimental data, and δ_0 is the initial static deformation corresponding to external precompression, p_0. C and β depend on the base material and roughness topography such as asperity size, shape, and height distribution. As a result, a wide range of β is reported in the literature based on roughness distribution [42,43]. Theoretically, β for a contact between rough fractal surfaces is such that $\beta = 1/(1+H)$ in the interval $H \in (0, 1)$, where H is a Hurst exponent [42]. Physically, β tends to be towards unity for roughness having statistical (or nonuniform) height distribution, whereas it tends to 0.5 for uniform roughness [41]. Further, the value of β for a rough contact changes if the asperities undergo plastic deformation; this has been experimentally observed, but only during the first loading cycle [40]. We use β corresponding to elastic deformations of rough contacts after the first loading cycle (i.e., after hysteresis has been removed) and consider wave amplitudes much smaller than the maximum deformation of asperities caused by the loads in the experimental work of [40]. Therefore, the rough contacts in our study do not undergo any plastic deformation during wave propagation and as a result, energy dissipation at the contacts is neglected.

In addition to the nonlinear relation of Eq. (1), the contacts exhibit strong nonlinearity when unloaded externally. For such *initially uncompressed* rough contacts, the relationship for compressive loads exhibits *essential* nonlinearity as

$$p(\Delta u) = [(1-\beta)C\Delta u]^{1/(1-\beta)}. \tag{2}$$

Here, we consider $C = 6\times10^{10}$ $\sqrt{\text{Pa}}/\text{m}$ and exponent $\beta = 0.5$, which results in a quadratic dependence of pressure on

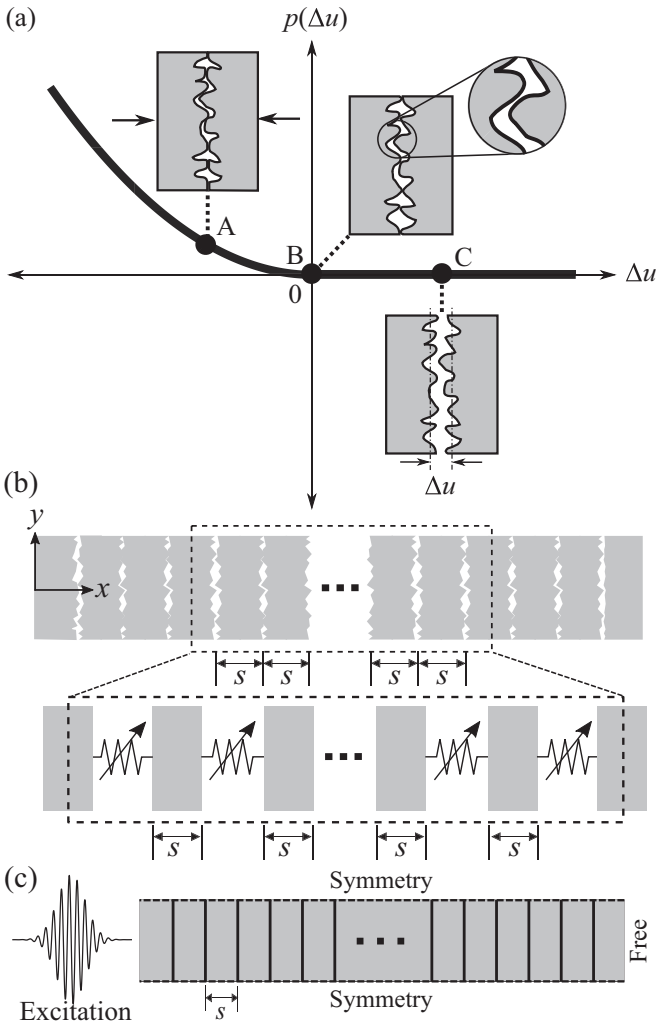

FIG. 1. Continuum phononic material with strongly nonlinear periodic rough contacts. (a) Strong nonlinearity of rough contacts arising from nonlinear dependence between contact pressure, $p(\Delta u)$, and displacement, Δu, and lack of tensile forces during contact loss. Markers highlight three contact configurations: (A) contact under compressive load undergoing flattening of rough asperities, (B) contact under no load, and (C) contact loss. The inset of (B) shows undeformed rough asperities, and thin black lines in (C) indicate nominal surfaces. (b) Phononic material with identical linear elastic layers coupled through rough contacts and corresponding schematic with contacts modeled as nonlinear springs. (c) FE model of phononic material in (b). The gray shaded region is a continuum, while vertical black lines are thin elastic layers (see text) representing contacts. Dashed lines are symmetric boundaries. A Gaussian tone burst is excited from the left boundary.

displacement, a similar approximation made in [44] owing to experimentally acquired data [41]. This means the rough contact model in our study corresponds to rough surfaces with uniform height distribution of asperities. Thus, the complete nonlinear force-displacement relation at the rough contacts in our system is

$$p(\Delta u) = \begin{cases} 0, & \Delta u > 0 \\ \frac{C^2 \Delta u^2}{4}, & \Delta u \leqslant 0. \end{cases} \tag{3}$$

This indicates that the dynamics of rough contacts is nonsmooth as contacting surfaces can collide and separate [Fig. 1(a)]. As a result, the dynamics of rough contacts are strongly nonlinear (in fact, not even linearizable) when no precompression is applied. This strong nonlinearity is in addition to the nonlinear power-law interaction between rough asperities.

B. Phononic material with periodic rough contacts

We develop a 1D phononic material by periodically arranging strongly nonlinear rough contacts. As a result, the elastic layers are coupled through rough contact nonlinearity [Fig. 1(b)]. The layers are modeled as aluminum (Young's modulus = 69 GPa, Poisson's ratio = 0.33, density = 2700 kg/m^3) to align with prior experiments [40], and each layer has identical thickness, s. Both the layers and contacts are assumed to be infinite in the y direction. We study wavelengths of the order of layer thickness, and thus, unlike granular crystals, significant elastic deformation occurs in our system—both at the rough contacts and within the layers. To model these mechanical deformations, layers are considered as continuous material and contacts are treated as nonlinear springs with the pressure-displacement relationship as given by Eqs. (3).

We study nonlinear wave propagation using finite element time-domain simulations based on our previous work in a weakly nonlinear regime [39] but modified enough to capture strongly nonlinear responses. The commercial FE package COMSOL MULTIPHYSICS 5.6 with solid mechanics module is used. The 1D phononic material is modeled within a two-dimensional (2D) plane strain framework [Fig. 1(c)] by applying symmetry boundary conditions (BCs) on the top and bottom edges of the model. A phononic material with 200 layers was modeled with displacement excitation BC on the left edge and traction-free BC on the right edge of the material. However, the simulations were ended even before the wave reaches the right boundary to avoid the influence of any reflections. The contacts were modeled through nonlinear thin elastic layers (TELs)—in-built internal BCs that decouple adjacent layers through a springlike element following the characteristics of Eqs. (3). We used the mapped quad meshing with the quadratic serendipity shape function. The element size in the model is determined based on the minimum number of elements required to capture (1) wave propagation results and (2) elastodynamics effects of layers. To satisfy the first criterion, the element size in the model was kept eight times smaller than the smallest wavelength of interest [39], i.e., $\Delta x_1 = \lambda_0/8$, where λ_0 is the smallest wavelength. λ_0 is defined by the first free-free acoustic resonance of the layers, $f_{\text{free-free}}$ (i.e., the largest frequency of interest in the simulations) and the bulk (i.e., aluminum) phase velocity, c_0. To satisfy the second criterion, at least four elements per layer were ensured, i.e., $\Delta x_2 = s/4$. Thus, the element size, Δx, in our model is $\min(\Delta x_1, \Delta x_2)$. The direct time-dependent solver—PARDISO—with generalized α time stepping is used, and the Courant-Friedrichs-Lewy (CFL) number of 0.2 is considered to achieve convergence while solving the partial differential equations numerically [39]. The time step, Δt, according to CFL in our simulation is $\Delta t = \text{CFL} \times \Delta x/c_0$.

We assumed negligible damping in the model due to the metal material and short wave propagation distance. Further, diffraction was neglected as a plane wave is excited in our model.

We excited a Gaussian modulated longitudinal tone burst at a center frequency, f, from the entire left edge of the FE geometry [Fig. 1(c)]. This type of excitation is common in experiments at ultrasonic frequencies where internal rough cracks have been studied [38]. Further, the modulation ensures a narrow-band frequency excitation and therefore can reveal additional frequencies generated due to the contact nonlinearity (for example, acoustic resonances of elastic layers from harmonics as discussed in Sec. III A). The Gaussian modulated burst is defined as

$$G(t) = U \sin(2\pi f t) \exp\left[-\left(\frac{t-\zeta}{\sigma}\right)^2\right], \tag{4}$$

where U is displacement excitation amplitude, t is time, and σ and ζ are the Gaussian parameters controlling the length and mean of the time-domain tone burst, respectively (i.e., controlling the number of cycles in the tone burst and therefore the number of collisions of rough surfaces). We introduce a nondimensional frequency, Ω, which is obtained by normalizing the excitation frequency, f, by the first fixed-free resonance frequency of layers, $f_{\text{fixed-free}}$. All the numerical simulations in this paper were conducted at $\Omega = 0.52$, unless explicitly specified. This particular frequency is chosen for simulation as it allows us to capture the elastic deformation of the layers (and therefore the elastodynamic response of the layers due to strong nonlinearity of contacts) within a reasonable computational cost. All the simulations were conducted with $\zeta = 12.5/f$, $\sigma = 2.5/f$ and at an excitation amplitude, U, corresponding to strain, ϵ, of 1.25×10^{-6} in layers, unless explicitly specified.

III. STRONGLY NONLINEAR WAVE DYNAMICS

Our phononic material is a synthesis of strong nonlinearity of rough contacts and linear continuum. This design concept gives rise to enriched dynamic response including both localized and propagating dynamics effects. In particular, localized effects include spectral energy transfer through the activation of layer acoustic resonances, and propagating dynamic effects include the formation of localized (compact) traveling waves. In this section, we report these nonlinear observations and discuss the mechanics behind their emergence and existence.

A. Energy transfer through layer resonances

The interaction of the excited wave with rough contacts results in clapping (or breathing), which is a collision and separation of contacting rough surfaces. We first explain the mechanics of such collision and separation and then the complex wave dynamics arising from it.

Consider a wave cycle propagating from layer 1 to layer 2 [Fig. 2(a)] such that layer 1 is the first layer of the phononic material in the direction of excitation. The rough contact between these layers is at an uncompressed initial condition; thus, the deformation, Δu, of the nonlinear spring representing the contact is initially zero [Fig. 2(a1)]. A collision occurs at the contact when the spring deformation is less than zero; otherwise, contact separation will take place. As a result, only a fraction of a full-wave cycle is transmitted across the contact [Fig. 2(a)]. This fraction of the cycle consists of a portion of the compressive part of the wave cycle [Figs. 2(a2) and 2(a3)]. This can be explained as follows: When the displacement of the wave cycle increases from zero to its peak amplitude, the rough surface of layer 1 is forced to move toward the rough surface of layer 2, causing the contact spring to deform and transmit the forces across the contact [Fig. 2(a2)]. At the same time, layer 2 deforms under the action of transmitted force, causing the rough surface at the contact to move to the right. During the next part of the wave cycle from its peak amplitude to zero, the rough surface of layer 1 retracts, releasing the spring deformation. The forces are still transferred across the contact during this stage until the rough surface of layer 1 retracts to position δ to account for the deformation of layer 2 [Fig. 2(a3)]. At this instant, the spring is back to the uncompressed state. As the cycle progresses, the lack of tensile force at the contact results in a contact loss ($\Delta u > 0$), and the rough surface of layer 2 cannot be pulled back [Fig. 2(a4)]. It should be noted that the wave transmitted across the contact now propagates through layer 2 and thus moves the right boundary (or surface) of layer 2 further toward the right. As expected, the tensile part of the wave cycle further increases the gap between the two rough surfaces at the contact [Fig. 2(a5)]. At the end of the cycle, layer 1 stays at the original position whereas layer 2 has moved to the right from its original position [Fig. 2(a6)].

This same clapping-separation behavior is repeated with each cycle of the tone burst until the tone burst reaches its maximum amplitude [red marker in Fig. 2(b)]. Note that the strongly nonlinear behavior of the contacts cause a change in the position of subsequent layers [for example, layer 2; see Fig. 2(c), black line]. Also, recall that due to the Gaussian profile, the amplitudes of the later cycles of the tone burst are larger than the previous ones [refer to the Gaussian tone burst in Fig. 2(b)]. Thus, wave cycles of the tone burst can cause clapping as long as their amplitudes are larger than the gap between the contacting surfaces generated from the previous cycles [compare black and light blue lines of Fig. 2(c)]. Wave cycles beyond the maximum amplitude of the tone burst do not result in clapping, as they do not cause the rough surfaces to come in contact [wave cycles beyond the red marker in Fig. 2(c)]. This contact loss remains in place for all times due to the lack of external precompression and the system's inability to support any tensile forces [Figs. 2(d) and 2(e)]. The forces transmitted across the contact during tone burst interaction propagate through the phononic material and subsequently cause separation of surfaces at each contact [Fig. 2(d)].

Interestingly, the normalized displacement profile, $\overline{U}$, inside the first layer of the phononic material shows a harmonic response for all times after tone burst excitation [inset of Fig. 3(a)]. Similar observations are made in layer 2 [inset of Fig. 3(b)] and so on. The wavelet transform reveals that the frequency content of these harmonic responses is different from the tone burst excitation frequency of $\Omega = 0.52$. The frequency spectrum shows that these oscillations, in fact, correspond to the acoustic resonances of the corresponding layers. Layer 1 exhibits the first acoustic resonance under the

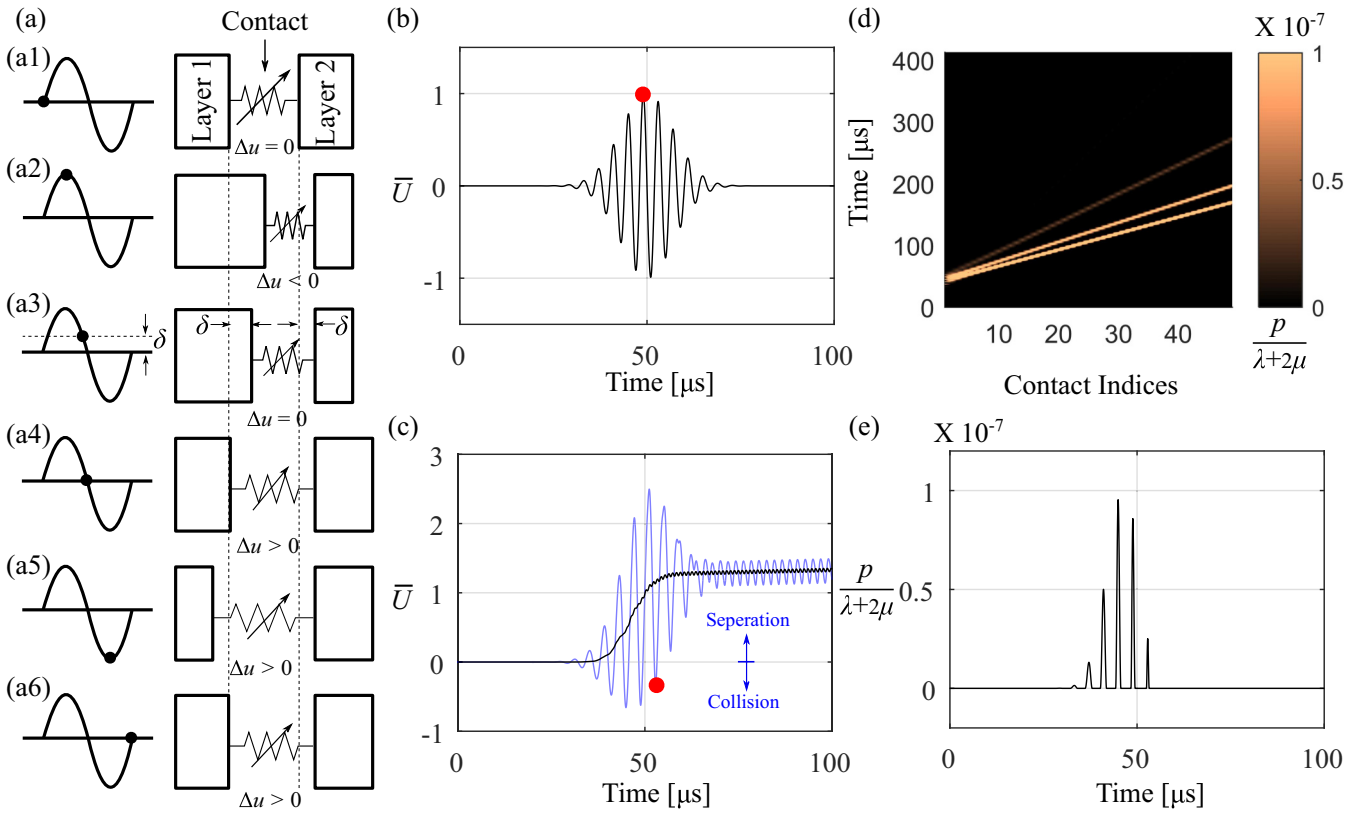

FIG. 2. Contact clapping under wave excitation. (a) Schematic demonstration of contact collision and separation under the first wave cycle of the Gaussian tone burst of (b). Black markers show specific instants of the wave cycle and corresponding contact conditions (a1)–(a6). Dashed lines are the initial interface location. The red marker in (b) is the maximum amplitude of the tone burst. (c) Displacement-time profile of the contact surface of layer 2 (black) and spring deformation of the rough contact between layers 1 and 2 (light blue). The last instance of clapping is associated with the maximum amplitude of the tone burst. The displacement profile, $\overline{U}$, is normalized by the excitation displacement amplitude, U. (d) Spatiotemporal plot of the contact pressure, and (e) temporal plot of the contact pressure at the first rough contact. Contact pressure is normalized by the uniaxial modulus of the layer material, where λ and μ are the material Lamé parameters.

fixed-free BC. This is because the tone burst interaction with the rough contact causes a separation between surfaces of layer 1 and layer 2 (as illustrated in Fig. 2), which ultimately creates a free BC on the right side of layer 1, and the excitation boundary is held fixed in its original position after the excitation (a physical BC as seen in the experiments [45]). These BCs of the layer activate acoustic resonances given by $nc_0/4s$, where n is the order of resonance, i.e., first, third, fifth, and so on. Thus, a fraction of the excited energy is now localized in layer 1 at its resonance frequencies. Higher-order resonances of this layer also exist but their amplitudes are much smaller than the first resonance. On the other hand, layer 2 experiences free BCs on either side because of loss of contact due to wave interaction with corresponding rough contacts. This results in acoustic resonances of layer 2 as given by $nc_0/2s$. Owing to free-free resonance, the center point inside layer 2 is a node while boundary points are antinodes [Fig. 3(d)]. Thus, wave responses shown in Fig. 3(b) are from a point close to the boundary in layer 2. Due to the separation of surfaces at each contact as waves propagate [Fig. 2(d)], the later layers also oscillate in a free-free resonance [discussed in terms of energy-frequency dependence later in Fig. 4(c)]; however, their amplitudes are very small due to relatively weaker excitation energy at later contacts.

This indicates that the combined effects of strong nonlinearity, continuum layers, and dynamic excitations result in the nonlinear energy transfer between frequencies. While many other nonlinear energy transfer mechanisms have been reported, such as subharmonic [46] and superharmonic [14,39] generation, self-demodulation [39,47], and nonlinear wave mixing [48], the mechanism in our phononic material is different in that it is fundamentally based on activating *acoustic* resonances of elastic elements (for example, layers in our case). This behavior has been not reported so far, as studies of unconsolidated phononic media were focused at frequencies much lower than modal frequencies of individual elastic elements (for example, particles in granular crystals [13,29]). At such low frequencies, elastic media between contacts have been considered point masses. As a result, there exists a lack of coupling between these masses after contact loss and no resonances are activated. While granular metamaterials [49] and woodpile structures [35] have shown spectral energy transfer through resonances, the mechanism is based on *local* resonances. These studies considered lumped-mass elements, where resonators are only coupled directly to an oscillator at each site. On the other hand, our system is not set up as a locally resonant system; in fact, the layers are coupled and modeled as continua. As a result, the resonances observed

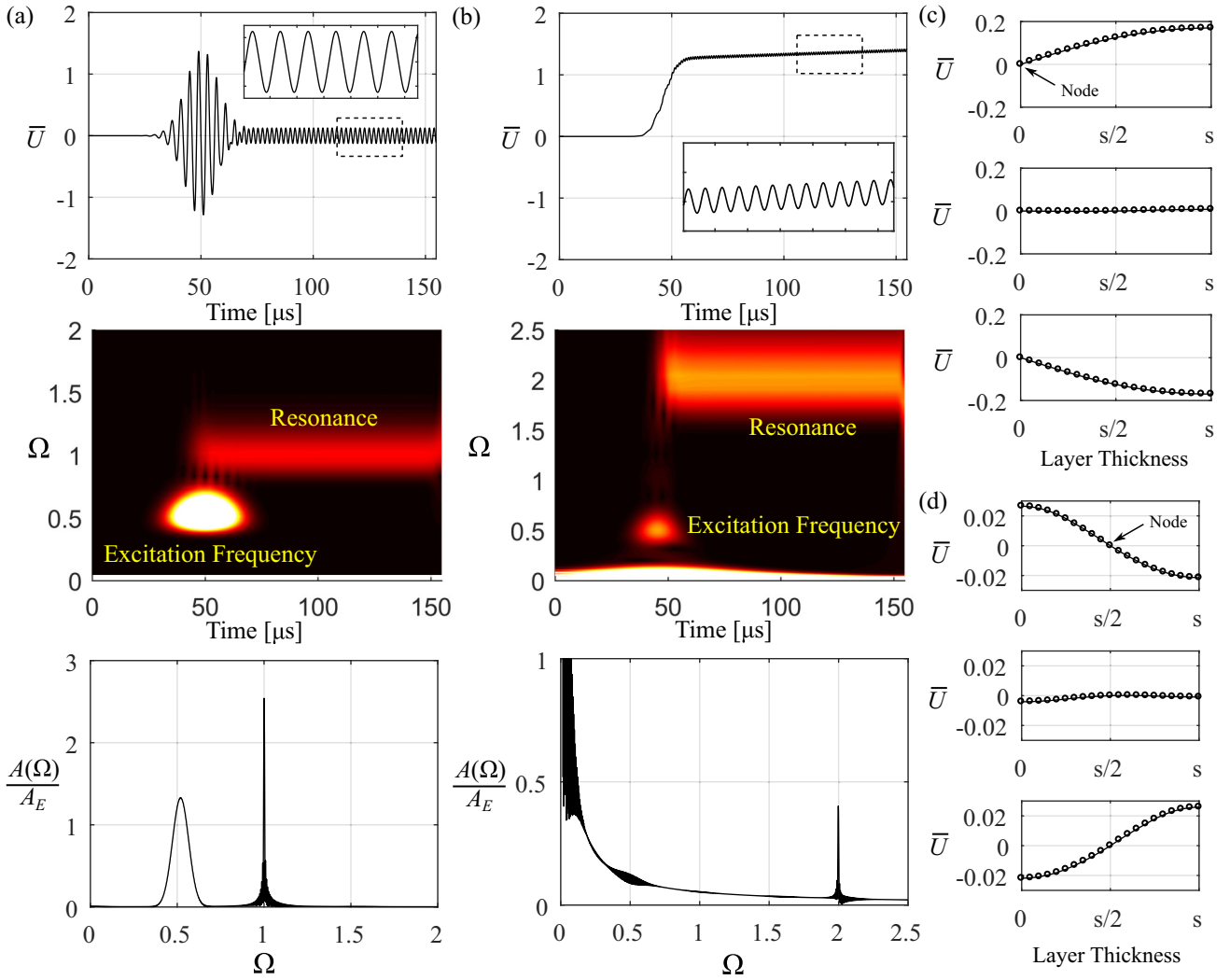

FIG. 3. Energy transfer through activated layer resonances due to strong contact nonlinearity. Dynamic response of (a) layer 1 and (b) layer 2. The response is extracted at the center point for layer 1 and near the contact boundary for layer 2. Time-domain normalized displacement (top), corresponding wavelet transform (middle), and fast Fourier transform (FFT) of the entire time-domain signal (bottom) are plotted for both the points. Insets are zoomed views of dashed rectangles indicating resonant oscillations. Wavelet amplitudes are normalized by their maximum amplitude whereas FFT amplitudes are normalized by the FFT amplitude of the excitation signal, A_E. Normalized modal deformations of (c) layer 1 and (d) layer 2 under fixed-free and free-free acoustic resonances, respectively. The deformations are plotted for three different time instants during resonant oscillations.

inside the phononic material correspond to acoustic resonances of these layers. Further, these acoustic resonances capture the physical deformation of the layers in the form of modes of finite bodies [Figs. 3(c) and 3(d)] and can also capture higher-order resonances of the layers for high frequency excitations.

We further evaluate the distribution and dependencies of the energies (normalized by the total energy, E_T) trapped in these layers due to their resonances on the excitation frequency, f (Fig. 4). We conduct parametric numerical simulations by sweeping excitation frequency from far away from the layer resonances to the layer resonance frequencies. As the excitation frequency approaches the resonance of layer 1, f_{r1}, almost all the energy of the system is stored in layer 1 [Fig. 4(a) as $f/f_{r1} \to 1$]. Interestingly, even when the excitation frequency is a fraction multiple of resonance frequency ($f/f_{r1} = 1/5, 1/4, 1/3, 1/2$), a significant portion of the total energy is stored in layer 1. This is because of higher harmonic responses arising from the nonlinear rough contact. As the wave interacts with the quadratically nonlinear rough contact, higher harmonics are generated at the contact, which activates the resonances of layer 1. Layer 1 stores more energy when lower-order harmonics, such as the second (for $f/f_{r1} = 1/2$) and third (for $f/f_{r1} = 1/3$), of the excitation frequency fall close to the resonance, compared to other higher-order harmonics (for $f/f_{r1} = 1/4, 1/5$). As expected, the energy stored in layer 2 also increases as the excitation frequency approaches the resonance of layer 2 [Fig. 4(b) as $f/f_{r2} \to 1$]. Similarly, fractional multiples of the excitation frequency contribute to activating the resonance of layer 2. Since harmonics with increasing order are associated with reduced amplitudes, the energies stored in layer resonances are increasingly weaker from harmonics with increasing order. For example, the free-free resonances of layer 2 activated for

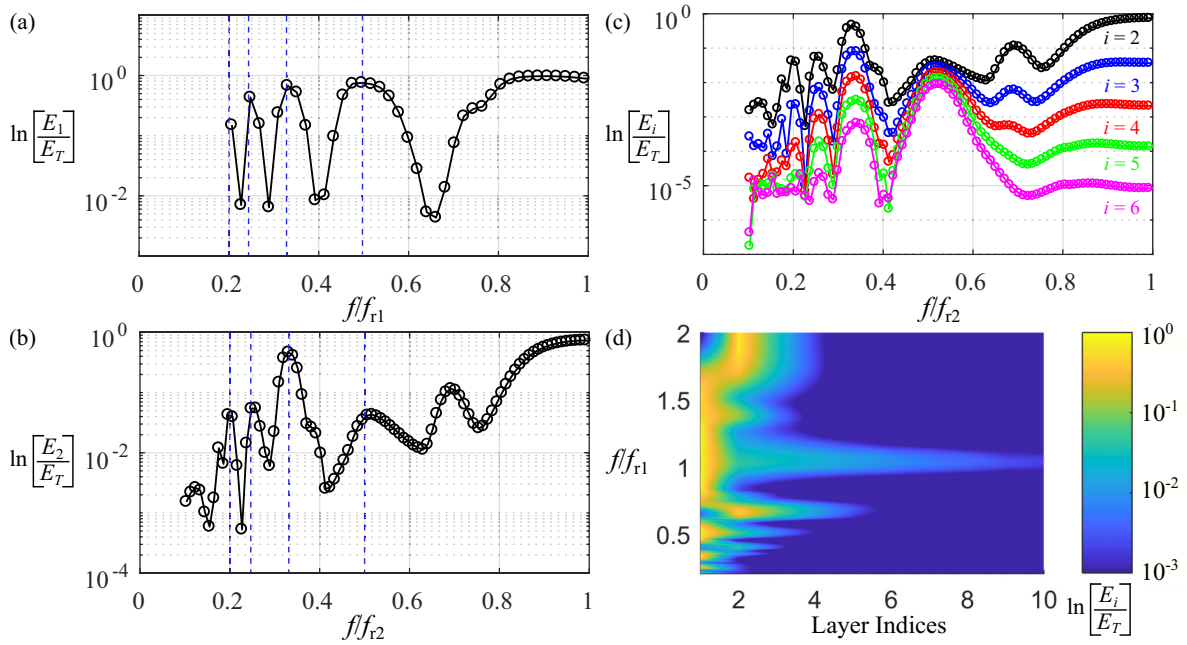

FIG. 4. Energy distribution within the phononic material due to layer acoustic resonances. Dependence of the energies trapped in (a) layer 1 (E_1) due to fixed-free resonance (f_{r1}) and (b) layer 2 (E_2) due to free-free resonance (f_{r2}) on excitation frequency, f. Vertical dashed lines correspond to when the excitation frequency is a fraction multiple of resonances. (c) Energy stored in the resonances of subsequent layers (E_i), where i indicates layer index from the excitation boundary. (d) Resonance energy distribution in the first ten layers of the phononic material for different excitation frequencies. The color bar indicates energy inside the layers normalized by the total energy in the system.

$f/f_{r2} \sim 0.125$ [leftmost peak in Fig. 4(b)] are much weaker than for other fractional frequencies; in particular, the energy in the layer resonance for $f/f_{r2} \sim 0.125$ is almost three orders of magnitude smaller than the total energy. As the excitation frequency decreases further ($f/f_{r2} \to 0$), corresponding higher-order harmonics become significantly less effective in exciting the free-free resonances of layer 2. At excitation frequency $f/f_{r2} \sim 0.7$, the generated third harmonic is close to the second-order free-free resonance of the layer ($2f_{r2}$). Thus, layer 2 stores more energy at this excitation frequency and shows a local maximum. The energy stored in layer 2 for an excitation frequency of $f/f_{r2} = 0.5$ is much smaller compared to other adjacent fractional frequencies. This is contradictory to the dependence of layer 1 energy on excitation frequency. This difference in the energy dependence of these two layers can be attributed to the relation between their resonance frequencies. Recall that the resonant frequency of layer 2, f_{r2}, is twice the resonant frequency of layer 1, f_{r1}. Thus, most of the total energy is localized in layer 1 when $f = f_{r1} = 0.5f_{r2}$, leaving only a small amount of energy in layer 2.

The energy dependence of the subsequent layers ($i = 3, 4, \ldots$) on excitation frequency is identical to layer 2 as all these layers oscillate under free-free resonance [Fig. 4(c)]. However, energy stored in these layers gradually reduces away from the excitation boundary [Fig. 4(d)]. While the reduction in stored energy with propagation distance is also frequency dependent, energy localization primarily happens in the first few layers ($i < 6$) only [Fig. 4(d)]. Clearly, a portion of the wave energy is localized in each of these layers as a wave propagates through them, specifically for frequencies that significantly contribute to activating the resonances of these layers. In other words, wave energy at these frequencies sharply reduces as it propagates. Therefore, wave interactions with subsequent contacts do not excite the resonances of the subsequent layers as effectively as previous layers. This can be seen through a monotonic reduction in the energy stored in layers with layer indices [Fig. 4(d)]. This is the reason for the reduction in the resonant oscillations of the later layers. The remaining portion of the total energy, which is not stored in these layers, propagates through the phononic material as we discuss in the next section (Sec. III B). Remarkably, the percentage of total energy propagating through the material is frequency dependent [Fig. 4(d)]. For example, the energy localized near the excitation boundary for $f/f_{r1} \sim 0.5$ and $f/f_{r1} \sim 1$ is almost the same as the total energy, whereas for $f/f_{r1} < 0.25$, $0.33 < f/f_{r1} < 0.5$, and $0.5 < f/f_{r1} < 0.6$, only a small portion of the energy is localized and the remaining energy propagates through the material. Clearly, the elastic media between nonlinear contacts contributes to complex dynamics due to overlapping effects of harmonic responses of contacts and resonances of layers. The energy dependencies presented here further inform that the proposed phononic material can be used for both acoustic attenuation and signal propagation by carefully selecting the excitation frequency with respect to layer acoustic resonances.

B. Propagation of stegotons

An interplay between nonlinearity and dispersion gives rise to solitary waves in periodic media [13,29]. A study of such waves in layered media with exponential material nonlinearity revealed a new type of solitarylike wave [36]. Unlike classical solitons, this new wave exhibited a roof- or ridge-type

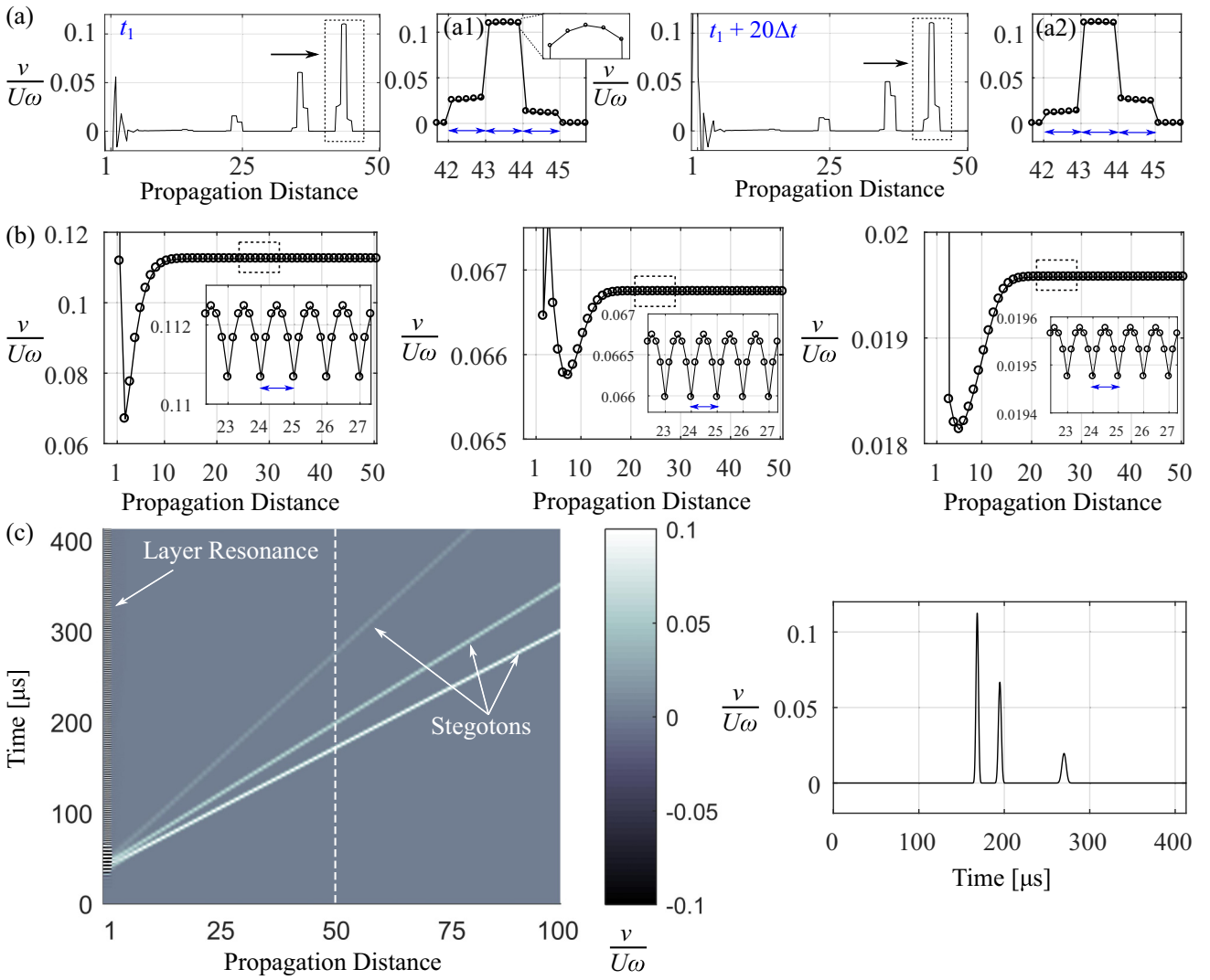

FIG. 5. Propagation of stegotons. (a) Formation of stegoton trains under tone burst excitation. Results at two different time instants, when stegotons are within the same layers, are shown indicating changing spatial profile of stegotons within these layers. Magnified views of the stegotons in dashed rectangles are to the right (a1 and a2). Layer width is marked with blue arrows. Inset of a1 shows stegoton amplitude variation inside a layer between the 43rd and 44th contacts. Arrows indicate wave propagation direction. Propagation distance is marked in terms of contact indices. (b) Stegoton amplitude dependence on propagation distance. The three plots correspond to the three stegotons of (a) with amplitudes evaluated at the center point in each layer. Insets show amplitudes evaluated at multiple locations inside each layer, in the neighborhood of the 25th contact (dashed rectangles), highlighting their local variation. The amplitudes are extracted from the temporal wave profile for each spatial point. Results are shown for the first 50 contacts only. (c) Spatiotemporal amplitude plot showing constant propagation speed of the generated stegotons. The temporal profile of the stegotons on the right corresponds to a location near the 50th contact (dashed vertical line).

spatial profile and thus was named a "stegoton." This wave, however, satisfied the other properties of solitons, which are propagation at a constant speed, and speeds being proportional to the wave amplitude. Later, stegotons were observed mathematically in the context of hyperbolic partial differential equations with spatially varying coefficients [50] and in a spring dimer configuration of Fermi-Pasta-Ulam-Tsingou lattices [51]. Still, it is not well understood what role nonlinearity plays in the propagation characteristics of stegotons. Moreover, stegotons have not been reported in a phononic system with physically motivated nonlinearity, such as contact nonlinearity. In our phononic materials, the combined effects of strong nonlinearity of rough contacts, dispersion from their periodic arrangement, and presence of elastic layers give rise to the propagation of stegotons. In this section, we report these waves and their characteristics in our phononic materials.

For a tone burst at excitation frequency, $\Omega = 0.52$, trains of stegotons are observed [Fig. 5(a)]. Such trains are generated because of two simultaneous effects: (1) multiple collisions of contacting rough surfaces due to multiple wave cycles in the tone burst excitation, and (2) layer internal reflections (such as seen in the dynamics of an impact of a striker on a Hopkinson bar [52]). Three dominant stegotons observed in the simulations are a result of three strong collisions of rough surfaces during the tone burst interaction with the first rough contact [Figs. 2(c) and 2(e)]. The loss of contact after

these collisions results in a gap between the layers preventing any further collision from the later cycles of the tone burst [Fig. 2(c)]. Additional stegotons due to other weaker collisions from tone burst cycles and internal layer reflections are also generated but their amplitudes are relatively negligible (two orders smaller).

The stegotons in our phononic materials are localized traveling waves yet due to the continuum between successive nonlinear contacts, they show a stepwise wave profile [Fig. 5(a)] that is different from the continuous shape of classical solitons. This is because displacements are discontinuous across the contact, causing steps in the spatial profile, whereas displacements inside layers vary smoothly due to layer deformation. This stepwise profile that consists of both jumps and continuous variation has not been seen in solitary waves in granular crystals, as these systems have thus far been modeled as spring-mass chains. Further, the stegoton spatial profiles continuously change while propagating through a collection of three layers, as can be seen at two representative time instants [Fig. 5(a)]. Note that the stegotons are propagating through the same three layers at both of these time instants. At t_1, the leading part of the stegoton (between 44th and 45th contact) is lower compared to the trailing part (between 42nd and 43rd contact) [Fig. 5(a1)]. The opposite is the case at $t_1 + 20\Delta t$ [Fig. 5(a2)]. The same change in profile is repeated as the wave propagates to the next layers. Clearly, two simultaneous effects are happening inside the phononic material: (1) macroscopic dynamics of phononic material and (2) localized dynamics within the layers. By macroscopic dynamics, we mean the dispersion from periodicity that counteracts that of the contact nonlinearity, which gives rise to the propagation of compact waves. This is similar to the mechanics of the formation of solitary waves in, e.g., nonlinear granular media. As a result, stegotons propagate with a constant spatial profile between layers despite exhibiting changing profiles within a collection of three layers. Additionally, the local dynamics of the continuum layers cause elastic deformations [inset of Fig. 5(a1)]. These localized effects have typically not been considered in nonlinear granular media, where masses are modeled as point masses. In that case, the displacement profile across the particles is constant, and no local effects are seen [13,29].

The spatial width of the stegotons in our phononic material is equal to three layers [Fig. 5(a)]. This is in contrast to the spatial width of solitary waves arising due to Hertzian contact nonlinearity, which is equal to five particle diameters [13], and due to exponentially nonlinear bilayer media, which is equal to ten layers [36]. As demonstrated in [53], the width of a solitary wave in granular crystal in terms of the particle size depends upon the coefficient resulting from the power law of contact nonlinearity. Solitary wave width narrows as the exponent of power-law nonlinearity increases. Based on this theory, it can be determined that the rough contact nonlinearity between elastic layers generates more compact localized waves compared to other forms of nonlinearities explored thus far.

The amplitudes of the stegotons, in terms of particle velocity, v, normalized by $U\omega$ (where ω is angular excitation frequency such that $\omega = 2\pi f$, and U is the excitation displacement amplitude), varies within the layer [insets of Fig. 5(b)] yet remains constant with propagation distance for a given point inside each layer. Note that the amplitudes shown in Fig. 5(b) are evaluated at the center point inside each layer, whereas amplitudes in the insets are evaluated at five locations inside each layer. Interestingly, these waves propagate at a constant speed when traced at a particular point [e.g., the center point in Fig. 5(c)] in each layer. The temporal profile highlights that the temporal width of these localized traveling waves is inversely proportional to their amplitude [Fig. 5(c)].

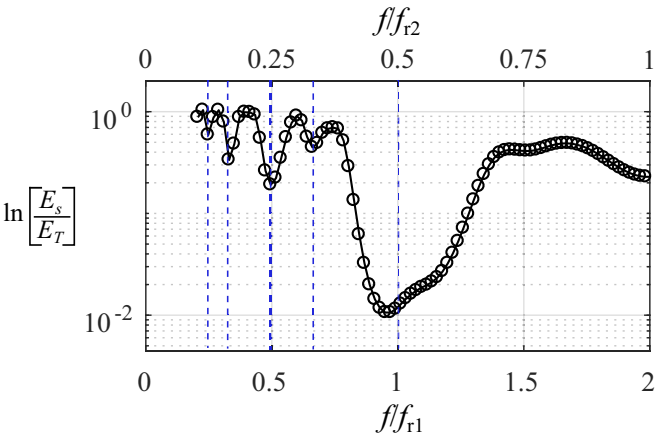

FIG. 6. Dependence of the energies carried by stegotons, E_S, on the excitation frequency, f. Vertical dashed lines correspond to when the excitation frequency is a fraction multiple of layer resonances.

Next, we analyze the energy carried by these stegotons (normalized by the total energy, E_T) as a function of excitation frequency, f (Fig. 6). The plotted energies, E_S, are of all the stegotons such that $E_S = \sum_1^k E_{Sk}$, where k is the number of stegotons generated in the phononic material. We observe that there exist certain frequencies for which stegotons carry very low energy (two orders smaller than the total energy), for example, $f/f_{r1} \sim 1$. This is because most of the total energy at these excitation frequencies is localized in layer 1 (refer to Fig. 4). Similarly, when the excitation frequency is a fraction multiple of the layer resonances, there exists a drop in the energy carried by the stegotons (refer to the dashed vertical lines in Fig. 6). For all other frequencies, stegotons carry a large portion of the energy through the phononic material. This characteristic demonstrates possible applications of this phononic material from filtering to signal propagation. This is because only a small amount of energy propagates through the material for certain frequencies (specifically for $f/f_{r1} \sim 1$) while for others, excited wave energy can travel through the material.

We further evaluate the dependence of stegoton propagation speed (c) on stegoton amplitude (v) [Fig. 7(a)], and on the contact pressure between layers (p) [Fig. 7(b)]. These relationships are determined at the excitation frequency of $\Omega = 0.52$. A long tone burst ($\zeta = 50/f$ and $\sigma = 10/f$) was used to generate multiple stegotons to find both the c-v and c-p relation. Stegoton amplitudes are evaluated at the center point in the 50th layer and the speed is determined through propagation time delay between two points separated by a distance equal to five layers. The dependence of the speed of stegotons on their amplitudes is found to be a power-law

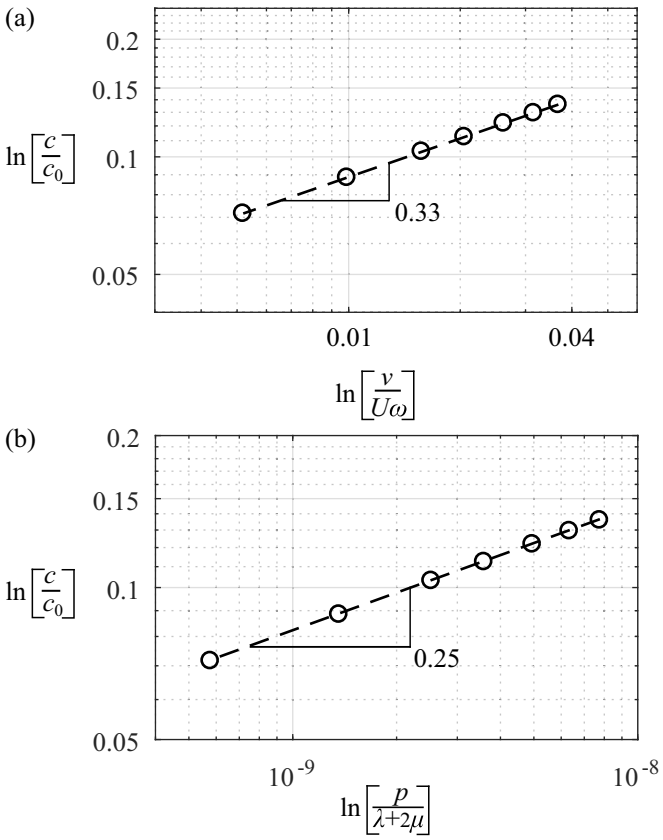

FIG. 7. Stegoton characteristics due to rough contact nonlinearity. Stegoton wave speed dependence on (a) its amplitude and (b) contact pressure. Dashed lines are linear fits of the normalized variables in logarithmic scale. Solid lines indicate slopes of the fitted lines along with corresponding values.

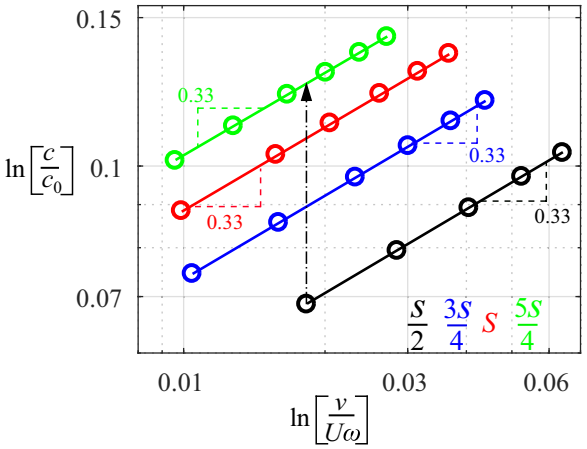

FIG. 8. Stegoton wave speed dependence on its amplitude for different layer thicknesses ($s/2$, $3s/4$, s, and $5s/4$). Dashed lines indicate slopes of the fits (solid lines) along with corresponding values. The arrow shows that speeds increase with layer thickness for a given amplitude.

relation with an exponent equal to $\sim 1/3$ [Fig. 7(a)]. The dependence of the speed of stegotons on the contact pressure follows a power-law relation with an exponent equal to $\sim 1/4$ [Fig. 7(b)].

It is interesting to compare these results to those of stegotons and solitary waves studied in prior work. For example, the dependence of the speed of stegotons on their amplitudes was found to be linear in a bilayer material with exponential nonlinearity [36]. These differences in dependencies potentially arise from the differences in the phononic materials of [36] and in this work, which are the form and type of nonlinearity (material vs contact), nature of nonlinearity (exponential vs quadratic), type of excitation (pulse vs tone burst), and impedance mismatch at the interfaces. In the case of Hertzian contact nonlinearity, the solitary wave speed has a power-law dependence on its amplitude with an exponent equal to 1/5 and on contact force between particles with an exponent equal to 1/6 [13]. Clearly, the phononic material with rough contact nonlinearity shows a stronger relationship between (1) the speed and amplitude of the stegotons and (2) the speed of stegotons and contact pressure, compared to Hertzian contact.

Further, the wave speed of stegotons can be tuned through system parameters, such as excitation amplitude, frequency, and layer thickness. As discussed in Fig. 7(a), the stegoton speed is proportional to its amplitude. Thus, the speed of stegotons can be tuned by controlling the amplitude of the generated stegotons. This can be achieved by changing the excitation amplitude: a larger excitation amplitude causes stronger collisions at the rough contacts forming stegotons with higher amplitudes, and vice versa. Similarly, as discussed in Fig. 6, the amount of energy carried by the stegotons depends upon the frequency of excitation. In other words, the properties of stegoton propagation (i.e., their amplitude and wave speed) can be changed by changing the excitation frequency. The speed of stegotons also depends upon the layer thickness. We evaluated the speed-amplitude relation of stegotons by following the method of Fig. 7(a) but for different layer thicknesses. For all the simulated cases, excitation frequency was appropriately selected to account for the change in layer resonances frequencies, i.e., to keep normalized frequency ($\Omega = 0.52$) the same. Increasing the layer thickness in phononic material increases the wave speed of the stegotons for a given amplitude; however, the relationship between the speed and amplitude remains unchanged (Fig. 8). This is likely because the relationship is governed by contact law, which depends only on the contacts and not the layer thickness. However, changing the layer thickness changes the overall dispersion and thus affects the speed of the stegotons. Finally, stegotons are generated from the counterbalance between nonlinearity and dispersion; hence, their speed-amplitude relation would depend upon the exponent of rough contact law. Rough contacts with different power-law exponents are achievable through different roughness topographies between contacting layers [41–43]. Therefore, stegoton properties can be potentially tuned through appropriate roughness selection as well.

C. Collision dynamics of stegotons

Studies of collision dynamics of solitary waves formed in granular crystals have shown that these waves escape frontal collision; however, they generate additional weaker solitary waves [54,55]. This is because the collision process releases

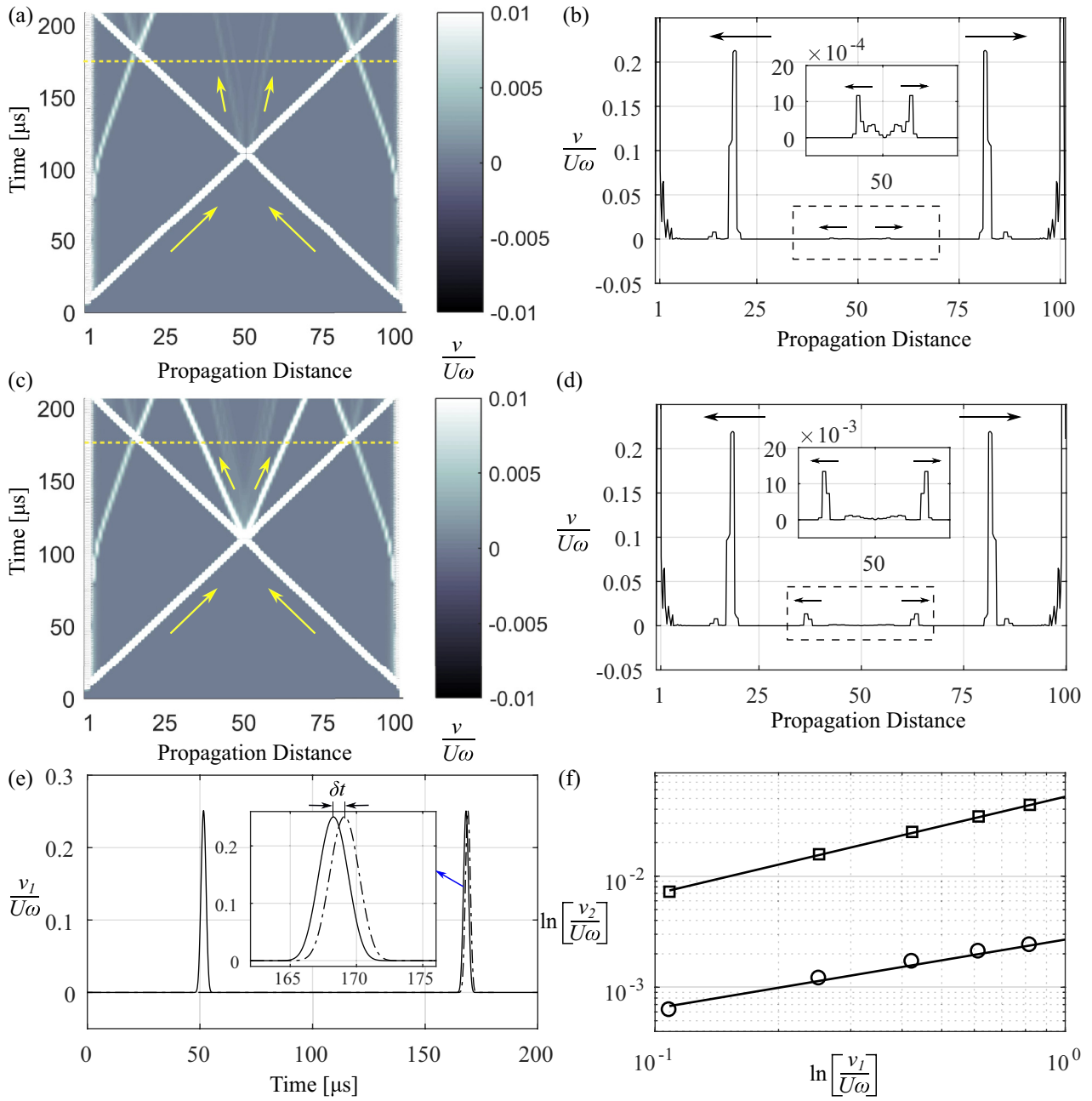

FIG. 9. Collision dynamics of stegotons. Spatiotemporal amplitude plot of stegotons when the collision happens (a) inside a layer (for an odd number of layers) and (c) at a rough contact (for an even number of layers). (b) and (d) are snapshots of (a) and (c), respectively, at time equal to 175 μs [dashed yellow line in (a) and (c)]. Arrows indicate the direction of propagation, with longer and shorter arrows corresponding to primary and collision-induced secondary stegotons, respectively. Insets in (b) and (d) are zoomed views of dashed rectangles. Propagation distances are in terms of contact indices. (e) Phase shift due to the collision of stegotons. Stegotons are recorded inside the 80th layer in the system with $N = 100$, when a stegoton is excited from each end (solid) and the left end only (dash-dotted). Inset is a zoomed view of the overlapped stegotons. (f) Dependence of the amplitudes of secondary stegotons, v_2, on primary stegotons, v_1, when the collision happens at a rough contact (squares) and inside a layer (circles).

some energy, owing to the squeezing of solitary waves during a collision, which eventually contributes to the generation of secondary solitary waves [54]. Surprisingly, the collision of stegotons in layered material with exponential nonlinearity did not result in the generation of additional waves [36]. In contrast, here we show that the collision of counterpropagating stegotons of equal amplitude in phononic materials with rough contacts generates a train of secondary stegotons.

To study collision dynamics, we excite a tone burst ($\zeta = 2.5/f$ and $\sigma = 0.5/f$) from each end of the phononic material at frequency $\Omega = 0.52$ such that the excited signal results in a single dominant stegoton propagating from both ends towards each other. We study two cases of phononic material, with odd ($N = 101$) and even ($N = 100$) numbers of layers. In the case of an odd number of layers [Fig. 9(a)], the collision takes place inside the elastic layer at the center ($i = 51$) of the phononic

material. Upon collision, we observe the formation of secondary stegotons with an amplitude (and therefore speed) much (two orders) smaller than primary stegotons [Figs. 9(a) and 9(b)]. In the case of an even number of layers [Fig. 9(c)], the collision takes place at a rough contact (between $i = 50$ and $i = 51$). Generation of secondary stegotons is observed in this case as well; however, the amplitudes of these generated stegotons are significantly higher than the secondary stegotons from the collision inside the layer [Figs. 9(b) and 9(d)]. In both cases, we observe a phase shift in propagating stegotons postcollision [Figs. 9(e), results shown for an even number of layers case only]—an observation consistent with the collision dynamics of solitary waves in granular crystals [55]. We further evaluate the dependence of the amplitudes of secondary stegotons on the amplitudes of primary stegotons in both collision cases [Fig. 9(f)]. There is an order of magnitude difference between the amplitudes of secondary stegotons generated at contact and within a layer.

To understand the role of the number of layers on the generation of secondary stegotons, we study displacements and energies of the layers at and in the vicinity of collision. When the collision of stegotons takes place inside a layer, the layer does not move before, during, or after the collision [Fig. 10(a), refer to i_c]. On the other hand, adjacent layers first move towards the center layer and then away from it postcollision, resulting in a contact loss [Fig. 10(a), refer to i_{c-1} and i_{c+1}]. This is because the stegoton propagating from left to right forces the layer i_{c-1} to initially move to the right, which eventually ceases due to the stegoton propagating in the opposite direction. This backward (right to left) propagating stegoton, when coming through the collision, forces the same layer to move to the left. The reverse is the case for the layer i_{c+1}. Despite these surrounding motions, the center layer is always at rest. As a result, the total kinetic energy in the center layer ($i_c = 51$) is approximately zero, unlike adjacent layers ($i_{c-1} = 50$ and $i_{c+1} = 52$) [Fig. 10(c)]. However, there exists a nonzero potential energy inside the center layer, which is significantly larger than the potential energy in other layers [Fig. 10(c), red lines]. This excess potential energy is a result of the squeezing of the stegotons, equivalent to the squeezing of solitary waves in granular crystals [54], during the collision. This squeezing can be physically understood as follows: When two identical stegotons propagating towards each other collide, the layers that came in contact due to leading fronts of the stegotons start to move in the reverse direction due to repelling forces. At the same time, the trailing fronts of the stegotons are moving in the direction of the wave propagation, eventually causing them to squeeze. Note that stegotons have a spatial width of three layers and therefore the trailing front is not affected by the dynamics of the leading front for a certain duration of time, allowing such squeezing. The potential energy released from this dynamics, however, is temporarily transferred to the center layer during the collision [Fig. 10(c)] and thus only generates weaker secondary stegotons [Figs. 9(a) and 9(b)]. As stegotons propagate through the collision, they regain their kinetic energy [Fig. 10(c), refer to $i = 40$ and $i = 62$]. This can also be confirmed from the fact that the kinetic energy in the stegotons postcollision is only $\sim$0.005% smaller than that of the precollision ones.

When stegotons collide at a contact, both layers adjacent to the contact (i^- and i^+) change their position, causing separation of contacting surfaces postcollision [Fig. 10(b)]. This can be understood in the same way as the motion of the adjacent layers in an odd number of layers. The squeezing of the stegotons in this case also releases potential energy [Fig. 10(d)], which cannot be stored at an interface and needs to be released. The phononic material considered here can only support localized traveling waves; hence, the energy is released in the form of (secondary) stegotons [Figs. 9(c) and 9(d)]. We do observe some of this potential energy temporarily stored in the adjacent layers [Fig. 10(d), refer to $i = 50$ and $i = 51$]. The energy in the layers in the vicinity of the collision also shows an evolving difference pre- and postcollision [Fig. 10(d), refer to $i = 49$ and $i = 52$], which is likely because of the overlapping effects of the leading and trailing fronts of the forward- and backward-propagating stegotons. Eventually, the stegotons attain a stable energy [Fig. 10(d), refer to $i = 40$ and $i = 61$]. Specifically, we observe that the energy in the stegotons postcollision is 0.4% smaller than precollision, indicating a stronger percentage of energy being utilized during the collision for the generation of secondary stegotons, compared to the case with an odd number of layers. In the absence of contact nonlinearity, it is possible that the energy imbalances upon collision in the system of [36] were stored inside the layers and thus no secondary stegotons were seen. Clearly, the dynamics of stegotons in phononic materials with rough contacts not only depend on the contact nonlinearity and elastic layers, but they also depend on the finite dimensions of the phononic material that can result in complex collision dynamics.

IV. CONCLUSION

We numerically studied strongly nonlinear wave propagation through a continuum phononic material with periodic rough contacts. The wave response of the phononic material is a combined effect of strong nonlinearity of rough contacts, dispersive effects due to their periodic arrangement, nonlinear coupling of elastic layers, and the finite dimensions of the phononic material. The interplay of these features in our phononic materials at frequencies comparable to the modal frequencies of elastic layers activates acoustic resonances of layers and generates stegotons, which are localized traveling waves belonging to the family of solitary waves. Layer resonances allow spectral energy transfer and localization near the excitation boundary, while stegotons carry wave energy without dispersion as these waves propagate with constant speed and amplitude. We illustrated these nonlinear signatures by evaluating the interrelationship of excitation frequency, energy, wave amplitude, and propagation speed. Stegotons are generated from the counterbalancing effects of strong nonlinearity and dispersion, in addition to discrete nonlinearity embedded in a continuum. Due to the discrete nonlinearity in the form of rough contacts between continua, stegotons exhibit different propagation characteristics than those of solitary waves, which includes a stronger dependence between propagation parameters such as amplitude, speed, and contact pressure. Further, stegotons show local variations in their spatial profiles and amplitudes inside elastic layers. While

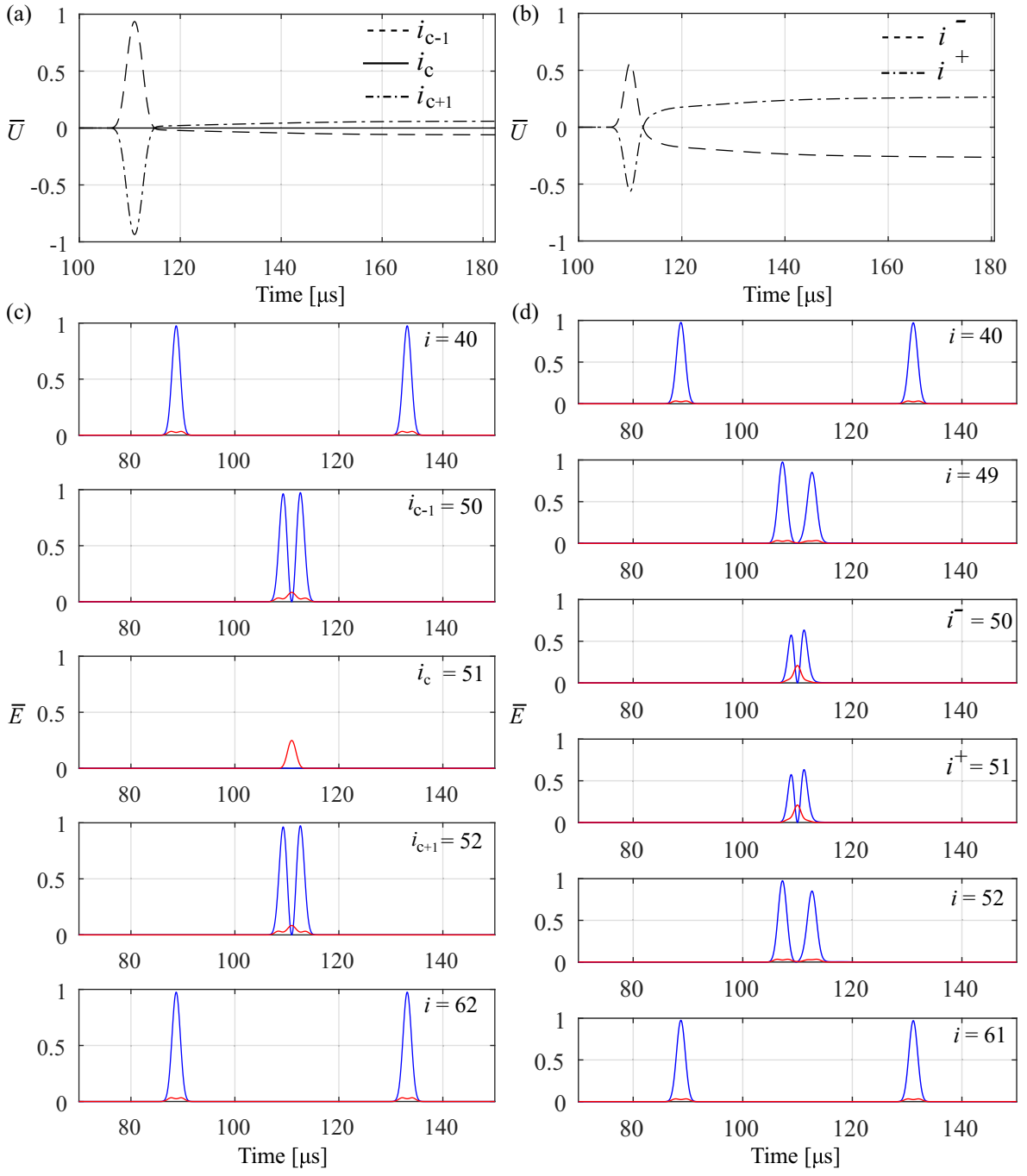

FIG. 10. Normalized displacement profile of the layers in the vicinity of collision in phononic material with an (a) odd and (b) even number of layers. For an odd number of layers, i_c is the layer index in which collision is taking place, while i_{c-1} and i_{c+1} are the layers before and after i_c, respectively. For an even number of layers, i^+ and i^- are the layers before and after the contact where collision is taking place. Signals are recorded at the center point inside layers. Normalized kinetic (blue) and potential (red) energy of the layers in systems with an (c) odd and (d) even number of layers. Energies, $\bar{E}$, are normalized by the total energy of the stegoton. The layer indices are located at the top-right corner of each subplot.

stegotons were formed at all the studied frequencies, propagation of energy through the phononic material was frequency dependent. Most of the energy either is spatially localized at frequencies close to (and fractional multiples of) layer resonances or propagates through the material as stegotons for other frequencies.

The observed nonlinear behaviors of the phononic material could have potential engineering applications. Layer resonances can localize energy near the excitation boundary, which can be used for impact mitigation, energy absorption, and harvesting. Further, stegotons can transfer signals over long propagation distances without dispersion in conservative material. This property could be potentially useful in developing advanced sensors and energy propagators. These properties are also amplitude and frequency dependent, and can be further tuned through system

parameters allowing control over the propagation of mechanical energy.

This study provides a platform to further explore phononic material with rough contacts for enriched dynamic response. The nonlinearity in these materials stems from the nonlinear mechanical deformation of the rough asperities in contacts. This would open opportunities to design a more robust and controllable nonlinear contact response by simply altering the roughness topography. While this study particularly focused on zero precompression, phononic materials with weak precompression can still exhibit strongly nonlinear dynamics for high excitation amplitudes and could possibly offer an advantage over tuning the wave response through external precompression. Importantly, strong nonlinear response of rough contacts, as studied here, may also allow the realization of new wave phenomena in damped media by overcoming dissipation losses typically not possible in soft-flexible metamaterials. The studied phononic material can be realized through a conventional manufacturing approach where layers can be aluminum discs or blocks with roughness on either side. Roughness could be generated through surface treatment using, e.g., rough sandpaper, shot peening, or sandblasting. Additive manufacturing can also be used to generate controlled roughness and height distribution of asperities. While aluminum is used as the base material in our study to align with prior experiments [40], one could certainly explore other materials, both hard and soft, that may change the nonlinearity at the contacts and thus the wave response.

The present study also opens directions in understanding the fundamental question: What is the role of discrete nonlinearity in wave propagation? The observations from our numerical simulations confirm that the existence of a continuum between successive and discrete nonlinearity can fundamentally change the overall dynamics of the system by introducing local modes and resonances. This work could spur interest in understanding the nature of energy exchange between coupled discrete-continuum nonlinear systems and may have implications on exploiting nonlinear discreteness to control wave propagation. Further, this concept is not just limited to mechanical systems but could be extended to other physics.

The emerging field of soft granular crystals cannot follow the assumption of conventional granular media where particles in contact are assumed as point masses. Our work provides groundwork on the nonlinear behavior of a system, qualitatively similar to that of soft granular crystals. This work opens additional questions in this field: What role does particle elastic deformation and resonance play on the overall dynamics of granular crystals? Which type of localized traveling waves do soft granular crystals support? Addressing these questions could help improve the dynamic response of soft granular media at frequencies close to the modal frequencies of individual beads.

Finally, we particularly focused on geomaterial-inspired rough contact nonlinearity; however, other physical sources such as hard-soft boundaries, laminated interfaces, and porosity are other examples of discrete nonlinearities in a continuum, and their role in wave propagation has not yet been explored in the phononics community. Specific to rough contacts, the role of friction, adhesion, and plasticity has been neglected in our study. The incorporation of these physical mechanisms could predict a more accurate, if not new, dynamic response. The heat generation at contacts and corresponding thermal stresses may change the local dynamic response of the material. Further, this study has been limited to wavelengths larger than the layer thickness and much larger than the rough asperities. The behaviors at much shorter wavelengths may have more pronounced and interesting dynamic effects. Extending the study to multidimensional systems could be exciting as it may shed light on the existence of vector stegotons.

ACKNOWLEDGMENTS

This work was supported by the Army Research Office and was accomplished under Grant No. W911NF-20-1-0250. The views and conclusions contained in this document are those of the authors and should not be interpreted as representing the official policies, either expressed or implied, of the Army Research Office or the U.S. Government. The U.S. Government is authorized to reproduce and distribute reprints for U.S. Government purposes notwithstanding any copyright notation herein.

[1] X. Yao and A. Belyanin, Phys. Rev. Lett. **108**, 255503 (2012).
[2] I. R. Epstein and K. Showalter, J. Phys. Chem. **100**, 13132 (1996).
[3] O. Bolmin, J. J. Socha, M. Alleyne, A. C. Dunn, K. Fezzaa, and A. A. Wissa, Proc. Natl. Acad. Sci. USA **118**, e2014569118 (2021).
[4] L. Zhang, J. Thingna, D. He, J.-S. Wang, and B. Li, Europhys. Lett. **103**, 64002 (2013).
[5] C. S. Wojnar, J.-B. le Graverend, and D. M. Kochmann, Appl. Phys. Lett. **105**, 162912 (2014).
[6] V. A. De Lorenci, R. Klippert, M. Novello, and J. M. Salim, Phys. Rev. D **65**, 063501 (2002).
[7] B. Gleich and J. Weizenecker, Nature (London) **435**, 1214 (2005).
[8] A. Rosario Hamann, C. Müller, M. Jerger, M. Zanner, J. Combes, M. Pletyukhov, M. Weides, T. M. Stace, and A. Fedorov, Phys. Rev. Lett. **121**, 123601 (2018).
[9] X. Zhao, G. Duan, K. Wu, S. W. Anderson, and X. Zhang, Adv. Mater. **31**, 1905461 (2019).
[10] G.-L. Dai, Front. Phys. **16**, 53301 (2021).
[11] V. F. Nesterenko, J. Appl. Mech. Tech. Phys. **24**, 733 (1983).
[12] R. K. Narisetti, M. J. Leamy, and M. Ruzzene, J. Vib. Acoust. **132**, 031001 (2010).
[13] V. F. Nesterenko, *Dynamics of Heterogeneous Materials* (Springer-Verlag, New York, 2001).
[14] V. Tournat, V. E. Gusev, V. Y. Zaitsev, and B. Castagnède, Europhys. Lett. **66**, 798 (2004).

[15] B. Liang, B. Yuan, and J. C. Cheng, Phys. Rev. Lett. **103**, 104301 (2009).
[16] F. Geniet and J. Leon, Phys. Rev. Lett. **89**, 134102 (2002).
[17] G. U. Patil and K. H. Matlack, Acta Mech. **233**, 1 (2022).
[18] J. S. Russell, Report of the 14th Meeting of the British Association for the Advancement of Science, 311 (1844).
[19] G. I. Stegeman and M. Segev, Science **286**, 1518 (1999).
[20] T. Heimburg and A. D. Jackson, Proc. Natl. Acad. Sci. USA **102**, 9790 (2005).
[21] S. Shrivastava, K. H. Kang, and M. F. Schneider, Phys. Rev. E **91**, 012715 (2015).
[22] B. Deng, P. Wang, Q. He, V. Tournat, and K. Bertoldi, Nat. Commun. **9**, 3410 (2018).
[23] A. Spadoni and C. Daraio, Proc. Natl. Acad. Sci. USA **107**, 7230 (2010).
[24] A. Leonard, L. Ponson, and C. Daraio, J. Mech. Phys. Solids **73**, 103 (2014).
[25] B. Deng, L. Chen, D. Wei, V. Tournat, and K. Bertoldi, Sci. Adv. **6**, eaaz1166 (2020).
[26] E. Kim, F. Restuccia, J. Yang, and C. Daraio, Smart Mater. Struct. **24**, 125004 (2015).
[27] C. Daraio, V. F. Nesterenko, E. B. Herbold, and S. Jin, Phys. Rev. E **72**, 016603 (2005).
[28] C. Daraio, V. F. Nesterenko, E. B. Herbold, and S. Jin, Phys. Rev. E **73**, 026610 (2006).
[29] G. Theocharis, N. Boechler, and C. Daraio, in *Acoustic Metamaterials and Phononic Crystals* (Springer, Berlin, 2013), pp. 217–251.
[30] F. Fraternali, G. Carpentieri, A. Amendola, R. E. Skelton, and V. F. Nesterenko, Appl. Phys. Lett. **105**, 201903 (2014).
[31] S. Katz and S. Givli, Extreme Mech. Lett. **22**, 106 (2018).
[32] B. Deng, J. R. Raney, V. Tournat, and K. Bertoldi, Phys. Rev. Lett. **118**, 204102 (2017).
[33] R. Ziv and G. Shmuel, Int. J. Non Linear Mech. **124**, 103502 (2020).
[34] I. V. Andrianov, V. V. Danishevs'kyy, O. I. Ryzhkov, and D. Weichert, Wave Motion **50**, 271 (2013).
[35] E. Kim, F. Li, C. Chong, G. Theocharis, J. Yang, and P. G. Kevrekidis, Phys. Rev. Lett. **114**, 118002 (2015).
[36] R. J. Leveque and D. H. Yong, SIAM J. Appl. Math. **63**, 1539 (2003).
[37] L. A. Ostrovsky and P. A. Johnson, Riv. Nuovo Cim. **24**, 1 (2001).
[38] D. Broda, W. J. Staszewski, A. Martowicz, T. Uhl, and V. V. Silberschmidt, J. Sound Vib. **333**, 1097 (2014).
[39] G. U. Patil and K. H. Matlack, Wave Motion **105**, 102763 (2021).
[40] B. Drinkwater, R. Dwyer-Joyce, and P. Cawley, Proc. R. Soc. London A **452**, 2613 (1996).
[41] S. Biwa, S. Nakajima, and N. Ohno, J. Appl. Mech. **71**, 508 (2004).
[42] R. Pohrt and V. L. Popov, Sci. Rep. **3**, 3293 (2013).
[43] C. Zhai, Y. Gan, D. Hanaor, G. Proust, and D. Retraint, Exp. Mech. **56**, 359 (2016).
[44] V. Aleshin, S. Delrue, A. Trifonov, O. Bou Matar, and K. Van Den Abeele, Ultrasonics **82**, 11 (2018).
[45] C. Kim, H. Yin, A. Shmatok, B. C. Prorok, X. Lou, and K. H. Matlack, Addit. Manuf. **38**, 101800 (2021).
[46] P. B. Silva, M. J. Leamy, M. G. Geers, and V. G. Kouznetsova, Phys. Rev. E **99**, 063003 (2019).
[47] V. Tournat, V. E. Gusev, and B. Castagnède, Phys. Rev. E **70**, 056603 (2004).
[48] F. Li, P. Anzel, J. Yang, P. G. Kevrekidis, and C. Daraio, Nat. Commun. **5**, 5311 (2014).
[49] L. Bonanomi, G. Theocharis, and C. Daraio, Phys. Rev. E **91**, 033208 (2015).
[50] D. I. Ketcheson, Ph.D. thesis, University of Washington, 2009.
[51] T. E. Faver, Ph.D. thesis, Drexel University, 2018.
[52] H. Kolsky, in *Stress Waves in Solids* (Dover, New York, 1963), pp. 87–91.
[53] D. Sun and S. Sen, Granular Matter **15**, 157 (2013).
[54] E. Ávalos and S. Sen, Phys. Rev. E **79**, 046607 (2009).
[55] F. Santibanez, R. Munoz, A. Caussarieu, S. Job, and F. Melo, Phys. Rev. E **84**, 026604 (2011).